Hindawi
Journal of Nanomaterials
Volume 2019, Article ID 6126031, 7 pages
https://doi.org/10.1155/2019/6126031

Research Article

Solid-Phase Hydrogen Storage Based on NH_3BH_3-SiO_2 Nanocomposite for Thermolysis

Joon-Hyung Jin, Seunghun Shin, and Jihoon Jung

Department of Chemical Engineering, Kyonggi University, 154-42 Gwanggyosan-ro, Yeongtong-gu, Suwon-si, Gyeonggi-do 16227, Republic of Korea

Correspondence should be addressed to Jihoon Jung; jhjung@kgu.ac.kr

Received 26 February 2019; Accepted 30 July 2019; Published 2 September 2019

Guest Editor: Nour F. Attia

Current H_2-proton exchange membrane fuel cell systems available for commercial applications employ heavy and high-risk physical hydrogen storage containers. However, these compressed or liquefied H_2-containing cylinders are only suitable for ground-based electric vehicles, because although highly purified H_2 can be stored in a cylinder, it is not compatible with unmanned aerial vehicles (UAVs), which require a lighter and more stable energy source. Here, we introduce a chemical hydrogen storage composite, composed of ammonia borane (AB) as a hydrogen source and various heterogeneous catalysts, to elevate the thermal dehydrogenation rate. Nanoscale SiO_2 catalysts with a cotton structure dramatically increase the hydrogen evolution rate on demand, while simultaneously lowering the startup temperature for AB thermolysis. Results show that the dehydrogenation reaction of AB with a cotton-structured SiO_2 nanocatalyst composite occurs below 90°C, the reaction time is less than a minute, and the hydrogen generation yield is over 12 wt%, with an activation energy of 63.9 kJ·mol^{-1}.

1. Introduction

Hydrogen—an abundant element in the universe—is a theoretically eco-friendly fuel and a clean energy source for fuel cells, as it produces no environmentally hazardous exhaust. Recent interest in hydrogen fuel has centered on how to safely store hydrogen with enhanced energy density. Essentially, there are two major hydrogen storage methods available: physical and chemical storage, where the latter includes sorbents, metal hydrides, and chemical hydrides [1]. Most commercially available hydrogen fuel cell-driven automobiles utilize physical storage, which is more reliable than chemical storage because pure hydrogen molecules are highly compressed, or even liquefied, to be stored in a physical storage tank. However, continuously raised safety concerns and the heavy weights of hydrogen fuel containers, which are absolutely incompatible with aerial vehicles, limit the employment of physical storage for some ground-based transportation vehicles.

Chemical hydrides store hydrogen fuel in various hydride forms such as sodium borohydride, alane, and ammonia borane (AB). These hydride compounds can be decomposed thermally or hydrolytically to generate H_2 gas. Although hydrolytic dehydrogenation of chemical hydrides occurs at temperatures lower than 80°C, the requirement of expensive catalysts for hydrolysis, the production of ammonia as a byproduct, and the low H_2 yield are practically incompatible with aerial vehicles [2–8]. Thermolysis of the chemical hydride does not require a noble metal catalyst and is relatively free of ammonia poisoning [9–11]. The H_2 yield through thermolysis of AB, which is a frequently employed hydride compound belonging to the chemical hydride group, can be increased up to 13 wt% [9]. In addition, a mixed approach has been introduced, involving a combination of both thermolysis and hydrolysis in series for the dehydrogenation of the AB-TiO_2 composite to enhance the hydrogen yield to the theoretical maximum [12]. Nevertheless, a high temperature requirement for the thermal dehydrogenation reaction and ammonia poisoning through trace amounts of water content in a reactor or reactants remain challenging.

In accordance with recent demands for unmanned aerial vehicles (UAVs) for aerial surveys, weather observations,

radio communication relays, and military purposes [13], here, we propose AB as a component for a disposable hydrogen fuel composite, which can be used for proton exchange membrane fuel cells (PEMFC). As an alternative energy storage device, a PEMFC powered by hydrogen fuel can immediately take advantage of the high efficiency of PEMFC (~50%) and high specific energy density of H_2 gas (~39,500 Wh·kg^{-1}). Indeed, a mechanically low-noise H_2-PEMFC system will perform better for a long-distance and low-altitude flight with UAVs than secondary lithium batteries, which are presently widely utilized, but commonly suffer from low energy density (~250 Wh·kg^{-1}) [14, 15]. Safe hydrogen storage and effective hydrogen generation on demand are of considerable importance in H_2-PEMFC power supply systems. Although some research on hydrogen storage/generation methods for PEMFC-based UAVs has been conducted [16, 17], a further enhanced energy density and highly efficient chemical hydride composite to reduce the weights of UAVs and effectively optimize PEMFC-based power pack systems are still required, especially for longer duration flights with UAVs [18–20].

AB contains 19.6 wt% of high hydrogen content per unit of mass. However, the thermal dehydrogenation temperature should be increased up to hundreds of degrees Celsius to obtain the theoretical maximum H_2 yield. Finding an appropriate catalyst to decrease the working temperature of the AB decomposition reaction with increased H_2 yield is of considerable importance. In this work, we present a characterization of a specifically designed chemical hydride composite, composed of AB and SiO_2 nanopowders (NP). Other researchers have reported on the availability of silicon-based catalysts, including quartz wool and mesoporous silica, in the thermal decomposition of AB. However, the actual working mechanism is not yet clearly understood [21–25]. Furthermore, the characteristics of the AB-SiO_2 NP composite are compared with those of other AB composites, containing various catalysts such as zeolites, metal, and metal oxide NP and boric acid (BA) as an additive. The optimization of the weight ratio between the AB and the catalysts is described, as well as the screening of the composites for fast H_2 evolution rate and low dehydrogenation temperature, to meet the demands of PEMFC-driven UAVs. Fourier transform infrared (FTIR) spectroscopy (ALPHA series, Bruker Corp.) is utilized to verify the hydrogen evolution of AB by thermolysis.

2. Materials and Methods

2.1. Catalyst Preparation and Reactor Design. Commercial zeolite ammonium ZSM-5 powder (CBV2314) is available from Zeolyst International (PA, USA). Laboratory preparation of the ZSM-5 in an attempt to remove tetrapropylammonium hydroxide (TPAOH) is as follows: Sodium aluminate dispersed in a basic aqueous medium is mixed in a flask with a basic Ludox® AS-40 colloidal silica suspension (40 wt% in H_2O) and stirred at room temperature for 3 h. Then, the suspended solution (the weight percentage of Si to Al is 67) is autoclaved at 190°C and 1.013 MPa for 12 h, and finally, the hydrothermally synthesized white powder-dispersed solution is filtrated and dried at 110°C overnight to produce the sodium-substituted TPAOH-free ZSM-5 catalyst (Na-ZSM-5). Na-ZSM-5 can be further stirred in a flask with ammonium nitrate at 80°C for 4 h. After filtration and drying at 110°C, the white product is calcined in an electric furnace at 600°C for 4 h to obtain hydrogen-substituted ZSM-5 (H-ZSM-5). The other materials and reagents are of analytical grade and purchased from Sigma-Aldrich (Milwaukee, USA), unless stated otherwise.

The laboratory-made hydrogen evolution reactor is composed of three thermocouples and a pressure gauge (Figures 1(a) and 1(b)). Thermocouple 1 directly measures the inside temperature of the vial that actually contains a fuel composite of AB and various catalysts and is feedback-controlled for precise control of the working temperature of the dehydrogenation reaction. Thermocouples 2 and 3 determine the temperatures of the inside and outside of the reactor, respectively, and the temperature difference between them gives the approximate energy loss of the reactor. The pressure gauge determines the amount of hydrogen gas generated by the heat-liberating AB dehydrogenation reaction.

2.2. Preparation of Fuel Composites. The weight of a fuel composite is 0.15 g. An AB : SiO_2 NP = 6 : 4 composite contains nine portions of AB (0.09 g) and six portions of SiO_2 NP (0.06 g). If the ratio were 8 : 2, then the composite would contain 0.12 g AB and 0.03 g SiO_2 NP. All reagent components are stored in a desiccator before use, to remove traces of water. After mixing both components gently in a 2 mL volume vial, the fuel composite is carefully placed in the reactor, followed by argon gas being blown into the reactor for 1 min. Then, the heating block increases the reactor temperature at a rate of 2°C min^{-1}.

2.3. Thermolysis of Ammonia Borane. The theoretical maximum H_2 yield from AB is 19.6 wt%: one-third of the hydrogen is generated at around 120°C, another third is dehydrogenated at around 160°C, and the final third requires over 500°C [26–28] (see Supplementary Material Fig. S1). Thermal dehydrogenation of AB can avoid the ammonia poisoning commonly observed in catalytic hydrolysis of AB, which generates one unit of ammonia for every three units of generated hydrogen. Even a level of ammonia of a few ppm can poison a PEMFC, depending on the exposure time to ammonia [29]. Although sodium borohydride ($d \approx 1.074$ g cm^{-3}) does not contain any amine or ammonia substituents and may provide a good alterative hydrogen fuel source without ammonia poisoning, the lighter AB ($d \approx 0.78$ g cm^{-3}) is a better energy source for aerial vehicles.

3. Results and Discussion

Various catalysts with an additive such as SiO_2 NP, aluminosilicate zeolites (CBV2314, H-ZSM-5, and Na-ZSM-5), Ni NP, metal oxides (ZrO_2, TiO_2, and Al_2O_3), and BA are compared in terms of the H_2 yield, reaction time, and onset reaction temperature for the thermal dehydrogenation of AB. The highly exothermic dehydrogenation reaction of AB

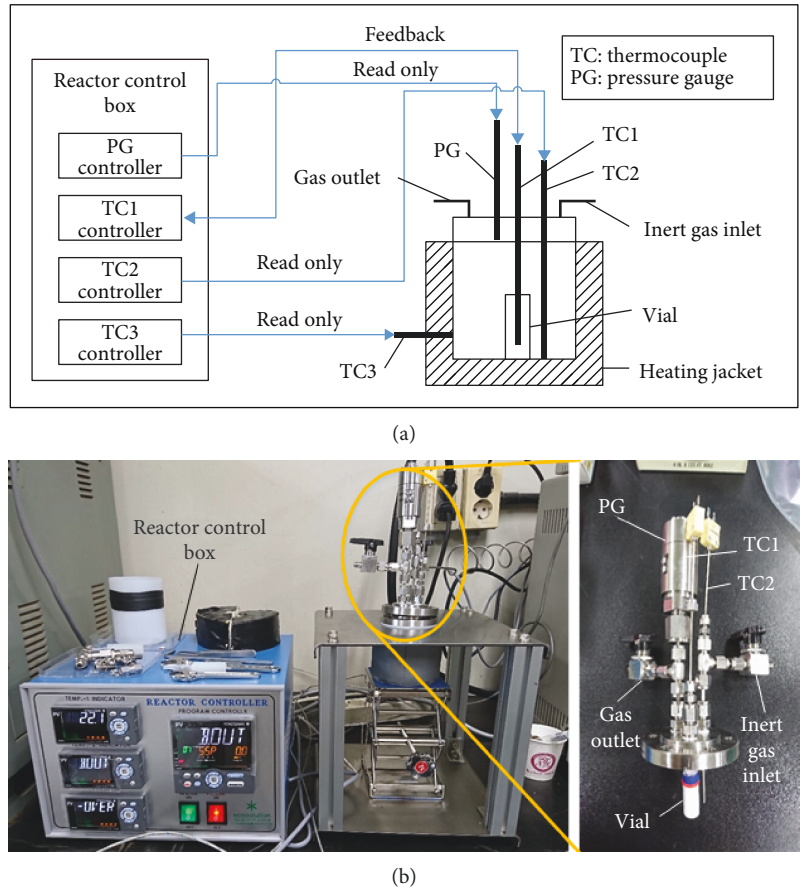

Figure 1: (a) Schematic drawing of the laboratory-made hydrogen evolution reactor, and (b) photo images. Note that the reactor is composed of three thermocouples, a pressure gauge (0–700 kPa), and the reactor controller box, which is interfaced with a PC. The inner volume of the reactor is approximately 44.6 mL.

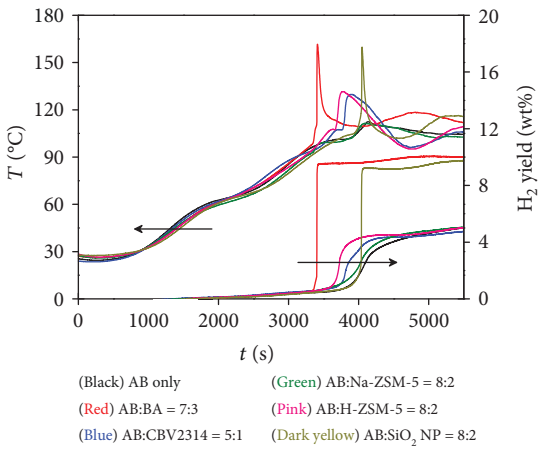

Figure 2: Thermolytic dehydrogenation of AB in the presence of various additives or catalysts. The set temperature is 100°C, and the heating rate is 2°C·min^{-1}. Dehydrogenation of AB is a strong exothermic reaction, and an increase in temperature is observed with H_2 gas evolution.

yields a sharp increase in temperature with the release of H_2 gas (Figure 2). As an additive, BA, which has achieved the best known thermal dehydrogenation performance for AB, produces a H_2 yield of 9.56 wt%. This means that a 2.15 mole of H_2 gas is generated for one mole of AB, based on the ideal gas equation of state, considering that the optimized weight ratio between AB and BA for the hydrogen evolution reactor employed in this work, shown in Figure 1, is 7 : 3.

The weight ratio optimization of the AB–BA composite is described in the Supplementary Material, Fig. S2. The mole-equivalent H_2 yield increases to 2.20 with the van der Waals equation, i.e., $(P + aN^2/V^2)(V - bN) = NRT$, where van der Waal constants a and b are 0.2453 bar·L^2·mol^{-2} and 0.02651 L·mol^{-1}, respectively. The higher the content ratio of the additives or catalysts in the hydrogen fuel composites, the faster the hydrogen evolution rate, and usually the lower the onset temperature of the dehydrogenation reactions. However, the H_2 yield as a weight percentage, defined by the weight ratio of hydrogen to the total weight of a composite, decreases as the amount of additive or catalyst in the composite increases. The onset temperature of the AB-BA composite is between 94 and 100°C, and the reaction time duration is less than 3 min. The AB-SiO_2 NP composite exhibits a H_2 yield of 9.26 wt% and a reaction time duration of 2 min, which are comparable with those of the AB-BA composite. While the temperature curve of the AB-BA composite exhibits a small shoulder peak directly before the abrupt temperature increase, the AB-SiO_2 NP composite

Table 1: Major catalytic parameters of additives and catalysts involved in the dehydrogenation reaction of AB via thermal decomposition.

Catalyst/additive (wt%)[a]	Onset temp. (°C)	H_2 yield (wt%)	Reaction time (s)
BA (30)	94	9.56	50
SiO_2 NP (20)	91	9.26	118
Na-ZSM-5 (20)	93	5.70	557
H-ZSM-5 (20)	95	5.70	433
CBV2314 (16.7)	94	4.75	749
No catalyst	98	5.05	588

[a]Content ratios are optimized for each additive or catalyst.

exhibits a single sharp peak. The other catalysts exhibit relatively large and wide shoulder peaks. Table 1 summarizes thermolytic parameters of the catalytic dehydrogenation of AB with various additives and catalysts. Only the thermolytic parameters of SiO_2 NP are comparable with those of BA, and the CBV2314 catalyst actually acts as an anticatalyst in AB thermolysis. The H_2 evolution curves of the other metal or metal oxide NP, including Ni, ZrO_2, anatase TiO_2, and Al_2O_3 are also provided (see Supplementary Material Fig. S3), but these exhibit poorer H_2 yields than that of SiO_2 NP, because the metal and metal oxides are significantly heavier and probably less porous than SiO_2 NP, as shown in Figure 3 and Supplementary Material Fig. S4.

In general, heat conduction mechanisms in powders and flake media differ from each other [30, 31]. Heat transfer in a heat conductor is similar to electron transfer in an electric semiconductor. Electron movement in randomly oriented bulk NP becomes faster through directional electron transfer [32, 33]. Similarly, a mechanical arrangement of AB-based fuel composite can allow a faster heat transfer rate in the in-plane direction of the composite. Effective heat transfer during the exothermic dehydrogenation of AB thermolysis enables enhanced hydrogen evolution compared with a simple powder-based AB composite. Hence, it can be assumed that a unidirectional compression force provides the AB-SiO_2 NP composite with a favorable orientation for better heat conduction in the fuel composite. Supplementary Material Fig. S5 illustrates how to prepare directionally favorable AB-SiO_2 NP composite. After gently mixing both components in a vial, the composite is carefully pressed from the top until only half of the original volume is left.

Even though the compositional optimization of the AB-SiO_2 NP composite shows that the 8 : 2 composite appears to provide the best H_2 yield with a minimized time requirement for a given amount of AB composite (Table 1), a greater H_2 yield can be obtained at a different optimized condition with the unidirectionally pressed AB-SiO_2 NP composite (Figure 4). Note that hydrogen gas is liberated even before the sharp temperature peaks are observed. A physically favorable arrangement of the composite increases the H_2 yield by over 20% and decreases the reaction time by approximately 50%. Table 2 summarizes the thermolytic parameters of various AB-SiO_2 NP composites.

The AB thermolysis reaction requires heat to initiate the dehydrogenation reaction, and the set temperature of the reactor strongly affects the H_2 yield, as shown in Figure 5. No reaction occurs at a set temperature of 50°C, meaning that the AB-SiO_2 NP composite is stable under normal atmospheric conditions. As the set temperature increases from 80 to 110°C, the reaction time and H_2 yield increase from 77 to 140 s and 10.37 to 11.67 wt%, respectively. Because a typical PEMFC system functions correctly at a working temperature of around 85°C, it would be reasonable to set the reactor temperature to approximately the same as the operation temperature of the PEMFC. Otherwise, additional equipment for insulation is required to thermally separate the PEMFC system from the hydrogen fuel supplier. The activation energy (E_a) of the SiO_2 NP-catalyzed dehydrogenation reaction of AB is 63.9 kJ·mol^{-1} (Supplementary Material Fig. S6). This is just one-third of the typical activation barrier of 180 kJ·mol^{-1} to the AB decomposition reaction [34].

Figure 6 shows the FTIR spectra of the AB-SiO_2 NP composite. Boron, nitrogen, and hydrogen atoms in a tetrahedral backbone with covalent single bonds lead to three characteristic FTIR bands for AB (Supplementary Material Fig. S7): the peaks observed in a range of 648–1822 cm^{-1} are assigned to B-N stretching vibrations, peaks between 2260 and 2820 cm^{-1} are assigned to B-H stretching vibrations, and N-H stretching modes are observed in a range of 3167–3712 cm^{-1} [21, 35, 36]. The evolution of hydrogen gas by heating the composite increases the bond order along the principal axis of AB. This means that the π-bond character becomes involved, in addition to the σ-bond character, and stretching frequencies are upshifted upon the bond order increase. More importantly, the B-H and N-H stretching intensities diminish when a large quantity of hydrogen gas is generated. As shown in Figure 6, both the B-H and N-H stretching intensities are considerably reduced after the thermal decomposition of AB, and the same result is observed with additive BA (Supplementary Material Fig. S7).

4. Conclusions

In this work, AB, a stable chemical hydride at room temperature and pressure, was thermally decomposed to produce hydrogen gas at a temperature of approximately 90°C, in the presence of SiO_2 NP. We designed our own hydrogen evolution reactor and hydrogen fuel composite to directly compare the results for the AB-SiO_2 NP composite with that of AB-BA, which has achieved the best thermolytic performance in other studies with a composite ratio of AB : BA of 8 : 2. The H_2 yield of the AB-SiO_2 NP composite (AB : SiO_2 NP = 7 : 3 in wt%) was 9.26 wt%, and the yield of the mechanically pressed one (8.5 : 1.5 composite in wt%) was 12 wt%, with a reaction time of less than a minute, which is comparable to that of the AB-BA composite. In general, chemical hydride-based hydrogen fuel composites for H_2-PEMFC for aerial vehicles should satisfy the following criteria: It should be sufficiently stable not to be dehydrogenated at a conventional atmospheric condition (<50°C), have a high capability for hydrogen storage to save

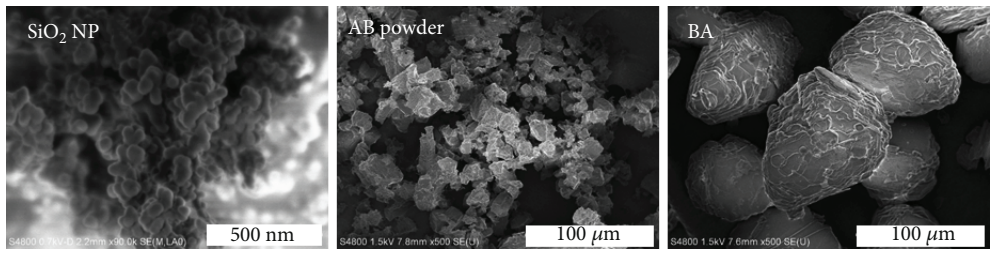

Figure 3: SEM images of the components of hydrogen fuel composites. SiO_2 NP shows much better porosity than those of AB and BA powders.

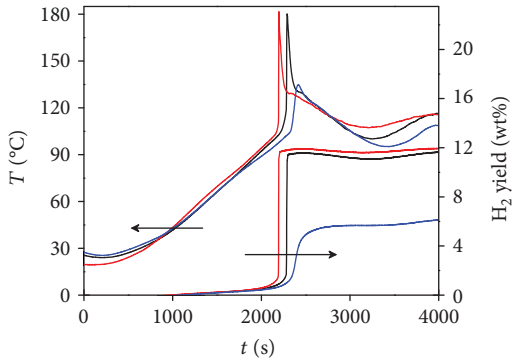

Figure 4: Hydrogen evolution curves and the catalytic parameters of various compositional ratios between AB and SiO_2 NP. The best result is obtained for the 8.5 : 1.5 composite, achieving 12.00 wt% H_2 yield, with a reaction time duration of less than 1 min.

Table 2: Hydrogen evolution parameters of various AB-SiO_2 NP composites in the dehydrogenation reaction of AB via thermolysis.

Composites	Onset temp. (°C)	H_2 yield (wt%)[a]	Reaction time (s)
AB : SiO_2 NP = 8 : 2	90	11.59	106
AB : SiO_2 NP = 8.5 : 1.5	89	12.00	48
AB : SiO_2 NP = 9 : 1	91	5.67	95

[a]1.0217 times increased by data fitting with the van der Waals equation instead of the ideal gas equation. Note that some harmful byproducts, e.g., NH_3 gas, may be included at an approximate level of thousands of ppm for each sample.

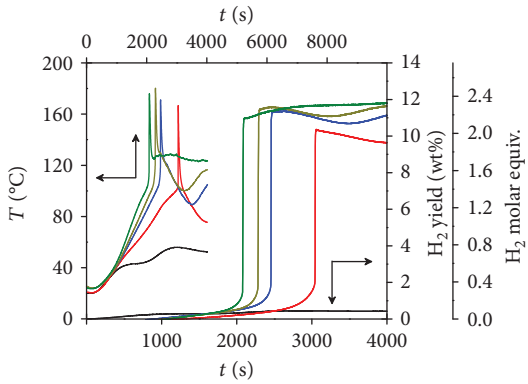

Figure 5: Hydrogen evolution curves at 50°C (black), 80°C (red), 90°C (blue), 100°C (dark yellow), and 110°C (green). The corresponding Arrhenius plot to measure the activation energy of the thermal dehydrogenation reaction of AB in the presence of the SiO_2 NP catalyst is also available (Supplementary Material Fig. S6). Note that mechanically pressed composites were employed, as shown in Supplementary Material Fig. S5, and the AB content in each composite is equal to 80 wt%.

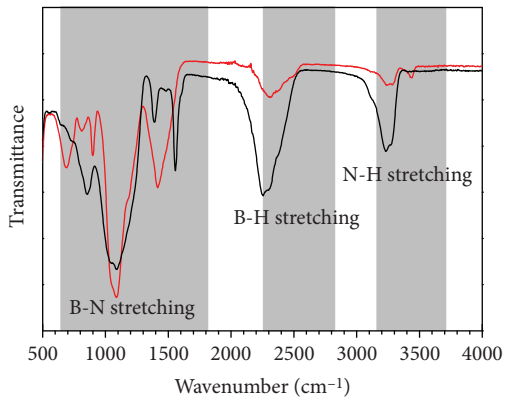

Figure 6: FTIR spectra of AB-SiO_2 NP composite before (black solid line) and after (red solid line) the thermal dehydrogenation reaction. H_2 gas evolution increases the bond order along the principal axis of AB. Therefore, the B-N stretching frequencies are upshifted, and the B-H and N-H stretching intensities decrease simultaneously.

weight, achieve a fast hydrogen evolution rate on demand at a temperature of less than 90°C, and have an in-built hydrogen fuel filtration system for the sake of ammonia-susceptible PEMFC (we did not seriously consider the by-product issue in the present work) [1]. The hydrogen evolution curves of the AB-SiO_2 NP composites showed that none of the compositional ratios investigated in this work thermally decomposed at a temperature below 50°C. Once the thermal dehydrogenation of AB occurred, the reaction ended within a couple of minutes. More precise optimization of the weight ratio between the two components, concerning not only compositional optimization but also the physical shape, density, and molecular orientation, could additionally enhance the hydrogen storage capability and

eventually reduce the total weight of a power generation package for UAVs. Given a thermally shielded fuel cartridge, the AB-SiO_2 NP composite could lead to the commercialization of disposable hydrogen fuel for UAVs.

Data Availability

The data used to support the findings of this study are included within the article. Additional information could be obtained from the supplementary materials.

Conflicts of Interest

The authors declare that there is no conflict of interest regarding the publication of this paper.

Authors' Contributions

The first and second authors contributed equally to this work.

Acknowledgments

This study was supported by the Agency for Defense Development (ADD) of Korea (Grant number 17-114-407-038).

Supplementary Materials

Fig. S1: TGA of pure AB. Thermal behavior of silica gel and SiO2 NP is also shown for comparison. Notable two peaks shown at 120 OC and 160 OC stems from formation of polyamidoboranes and/or polyimidoboranes by the AB decomposition. Note that a slight mass loss of silica gel and SiO2 NP is due to evaporation of the surface-adsorbed water vapor and unspecified polymeric contaminants. Fig. S2: the weight ratio optimization of the AB-BA composites. The onset temperature and the H2 yield of each composite are as follows, respectively: 94 OC and 8.21 wt% for AB : BA = 6 : 4 composites; 98 OC and 9.56 wt% for AB : BA = 7 : 3 composites; 100 OC and 5.55 wt% for AB : BA = 8 : 2 composites. Fig. S3: hydrogen evolution curves of AB composites containing various metal or metal oxide NP such as Ni (black), ZrO2 (red), anatase TiO2 (blue), and Al2O3 (green). H2 yield of each composite is 4.27, 7.44, 3.74, and 3.97 wt% in order. Note that AB content in each composite is the same as 60 wt%. Fig. S4: photo images (×1200) of various metal or metal oxide NP catalysts including Ni ($d \approx 8.91$ g cm^{-3}), ZrO2 ($d \approx 5.68$ g cm^{-3}), anatase TiO2 ($d \approx 3.8$ g cm^{-3}), and Al2O3 ($d \approx 3.99$ g cm^{-3}). Fig. S5: unidirectional compression of AB-SiO2 NP composite to reduce the volume by half. Fig. S6: Arrhenius plot based on the hydrogen evolution curves at 4 different temperatures shown in Figure 5. Note that the obtained E_a from the slope measures 63.9 kJ·mol^{-1}. Fig. S7: (a) FTIR spectra of AB flake and AB powder. Both spectra commonly show 3 characteristic bands, i.e., BN stretching, BH stretching, and NH stretching bands. (b) FTIR spectra of AB and BA composites before and after the thermal dehydrogenation reaction. Note that the BH and NH stretching peaks are simultaneously reduced after the dehydrogenation reaction. *(Supplementary Materials)*

References

[1] H. T. Hwang and A. Varma, "Hydrogen storage for fuel cell vehicles," *Current Opinion in Chemical Engineering*, vol. 5, pp. 42–48, 2014.

[2] C. Li, J. Zhou, W. Gao et al., "Binary Cu–Co catalysts derived from hydrotalcites with excellent activity and recyclability towards NH_3BH_3 dehydrogenation," *Journal of Materials Chemistry A*, vol. 1, no. 17, pp. 5370–5376, 2013.

[3] L. Cui, Y. Xu, L. Niu, W. Yang, and J. Liu, "Monolithically integrated CoP nanowire array: an on/off switch for effective on-demand hydrogen generation via hydrolysis of $NaBH_4$ and NH_3BH_3," *Nano Research*, vol. 10, no. 2, pp. 595–604, 2017.

[4] S. Akbayrak and S. Ozkar, "Ruthenium(0) nanoparticles supported on multiwalled carbon nanotube as highly active catalyst for hydrogen generation from ammonia-borane," *ACS Applied Materials & Interfaces*, vol. 4, no. 11, pp. 6302–6310, 2012.

[5] N. Sahiner and A. O. Yasar, "Imidazolium based polymeric ionic liquid microgels as an alternative catalyst to metal catalysts for H_2 generation from methanolysis of $NaBH_4$," *Fuel Processing Technology*, vol. 152, pp. 316–324, 2016.

[6] M. J. Valero-Pedraza, D. Cot, E. Petit, K. F. Aguey-Zinsou, J. G. Alauzun, and U. B. Demirci, "Ammonia borane nanospheres for hydrogen storage," *Acs Applied Nano Materials*, vol. 2, no. 2, pp. 1129–1138, 2019.

[7] N. Sahiner and F. Seven, "The use of superporous p(AAc (acrylic acid)) cryogels as support for Co and Ni nanoparticle preparation and as reactor in H_2 production from sodium borohydride hydrolysis," *Energy*, vol. 71, pp. 170–179, 2014.

[8] B. Coşkuner, A. Kantürk Figen, and S. Pişkin, "Solid state preparation and reaction kinetics for Co/B as a catalytic/acidic accelerator for $NaBH_4$ hydrolysis," *Reaction Kinetics Mechanisms and Catalysis*, vol. 109, no. 2, pp. 375–392, 2013.

[9] H. T. Hwang, P. Greenan, S. J. Kim, and A. Varma, "Effect of boric acid on thermal dehydrogenation of ammonia borane: H_2 yield and process characteristics," *AICHE Journal*, vol. 59, no. 9, pp. 3359–3364, 2013.

[10] J. Luo, X. Kang, C. Chen, J. Song, D. Luo, and P. Wang, "Rapidly releasing over 9 wt % of H_2 from NH_3BH_3–Mg or NH_3BH_3–MgH_2 composites around 85°C," *Journal of Physical Chemistry C*, vol. 120, no. 33, pp. 18386–18393, 2016.

[11] J. Luo, X. Kang, and P. Wang, "Synthesis, formation mechanism, and dehydrogenation properties of the long-sought $Mg(NH_2BH_3)_2$ compound," *Energy & Environmental Science*, vol. 6, no. 3, pp. 1018–1025, 2013.

[12] O. V. Komova, V. I. Simagina, N. L. Kayl et al., "Improved low-temperature hydrogen generation from NH_3BH_3 and TiO_2 composites pretreated with water," *International Journal of Hydrogen Energy*, vol. 38, no. 15, pp. 6442–6449, 2013.

[13] O. Gonzalez-Espasandin, T. J. Leo, and E. Navarro-Arevalo, "Fuel cells: a real option for unmanned aerial vehicles propulsion," *Scientific World Journal*, vol. 2014, article 497642, 12 pages, 2014.

[14] S. F. J. Flipsen, "Power sources compared: the ultimate truth?," *Journal of Power Sources*, vol. 162, no. 2, pp. 927–934, 2006.

[15] J. M. Tarascon and M. Armand, "Issues and challenges facing rechargeable lithium batteries," *Nature*, vol. 414, no. 6861, pp. 359–367, 2001.

[16] K. Kim, T. Kim, K. Lee, and S. Kwon, "Fuel cell system with sodium borohydride as hydrogen source for unmanned aerial

vehicles," *Journal of Power Sources*, vol. 196, no. 21, pp. 9069–9075, 2011.

[17] J. E. Seo, Y. Kim, Y. Kim et al., "Portable ammonia-borane-based H_2 power-pack for unmanned aerial vehicles," *Journal of Power Sources*, vol. 254, pp. 329–337, 2014.

[18] C. K. Dyer, "Fuel cells for portable applications," *Journal of Power Sources*, vol. 106, no. 1-2, pp. 31–34, 2002.

[19] J. H. Wee, "Applications of proton exchange membrane fuel cell systems," *Renewable & Sustainable Energy Reviews*, vol. 11, no. 8, pp. 1720–1738, 2007.

[20] Z. Liu, Y. Dai, Z. Zheng, and B. Huang, "Covalently-terminated germanane GeH and $GeCH_3$ for hydrogen generation from catalytic hydrolysis of ammonia borane under visible light irradiation," *Catalysis Communications*, vol. 118, pp. 46–50, 2019.

[21] H. T. Hwang, A. Al-Kukhun, and A. Varma, "High and rapid hydrogen release from thermolysis of ammonia borane near PEM fuel cell operating temperatures," *International Journal of Hydrogen Energy*, vol. 37, no. 3, pp. 2407–2411, 2012.

[22] H. T. Hwang, A. Al-Kukhun, and A. Varma, "High and rapid hydrogen release from thermolysis of ammonia borane near PEM fuel cell operating temperatures: effect of quartz wool," *International Journal of Hydrogen Energy*, vol. 37, no. 8, pp. 6764–6770, 2012.

[23] A. Gutowska, L. Li, Y. Shin et al., "Nanoscaffold mediates hydrogen release and the reactivity of ammonia borane," *Angewandte Chemie-International Edition*, vol. 44, no. 23, pp. 3578–3582, 2005.

[24] A. Paolone, O. Palumbo, P. Rispoli, R. Cantelli, T. Autrey, and A. Karkamkar, "Absence of the structural phase transition in ammonia borane dispersed in mesoporous silica: evidence of novel thermodynamic properties," *Journal of Physical Chemistry C*, vol. 113, no. 24, pp. 10319–10321, 2009.

[25] L. Q. Wang, A. Karkamkar, T. Autrey, and G. J. Exarhos, "Hyperpolarized ^{129}Xe NMR investigation of ammonia borane in mesoporous silica," *Journal of Physical Chemistry C*, vol. 113, no. 16, pp. 6485–6490, 2009.

[26] U. B. Demirci, S. Bernard, R. Chiriac, F. Toche, and P. Miele, "Hydrogen release by thermolysis of ammonia borane NH_3BH_3 and then hydrolysis of its by-product $[BNH_x]$," *Journal of Power Sources*, vol. 196, no. 1, pp. 279–286, 2011.

[27] T. Kobayashi, S. Gupta, M. A. Caporini, V. K. Pecharsky, and M. Pruski, "Mechanism of solid-state thermolysis of ammonia borane: a ^{15}N NMR study using fast magic-angle spinning and dynamic nuclear polarization," *Journal of Physical Chemistry C*, vol. 118, no. 34, pp. 19548–19555, 2014.

[28] L. Li, X. Yao, C. Sun et al., "Lithium-catalyzed dehydrogenation of ammonia borane within mesoporous carbon framework for chemical hydrogen storage," *Advanced Functional Materials*, vol. 19, no. 2, pp. 265–271, 2009.

[29] R. Halseid, P. J. S. Vie, and R. Tunold, "Effect of ammonia on the performance of polymer electrolyte membrane fuel cells," *Journal of Power Sources*, vol. 154, no. 2, pp. 343–350, 2006.

[30] C. J. Gomes, M. Madrid, J. V. Goicochea, and C. H. Amon, "In-plane and out-of-plane thermal conductivity of silicon thin films predicted by molecular dynamics," *Journal of Heat Transfer*, vol. 128, no. 11, pp. 1114–1121, 2006.

[31] C. Pohlmann, L. Rontzsch, S. Kalinichenka, T. Hutsch, T. Weissgarber, and B. Kieback, "Hydrogen storage properties of compacts of melt-spun $Mg_{90}Ni_{10}$ flakes and expanded natural graphite," *Journal of Alloys and Compounds*, vol. 509, pp. S625–S628, 2011.

[32] S. H. Kang, S. H. Choi, M. S. Kang et al., "Nanorod-based dye-sensitized solar cells with improved charge collection efficiency," *Advanced Materials*, vol. 20, no. 1, pp. 54–58, 2008.

[33] R. Jose, V. Thavasi, and S. Ramakrishna, "Metal oxides for dye-sensitized solar cells," *Journal of the American Ceramic Society*, vol. 92, no. 2, pp. 289–301, 2009.

[34] A. C. Gangal, P. Kale, R. Edla, J. Manna, and P. Sharma, "Study of kinetics and thermal decomposition of ammonia borane in presence of silicon nanoparticles," *International Journal of Hydrogen Energy*, vol. 37, no. 8, pp. 6741–6748, 2012.

[35] S. Frueh, R. Kellett, C. Mallery et al., "Pyrolytic decomposition of ammonia borane to boron nitride," *Inorganic Chemistry*, vol. 50, no. 3, pp. 783–792, 2011.

[36] J. Zhang, Y. Zhao, D. L. Akins, and J. W. Lee, "CO_2-enhanced thermolytic H_2 release from ammonia borane," *Journal of Physical Chemistry C*, vol. 115, no. 16, pp. 8386–8392, 2011.